Gas-Sensing Property of TM-MoTe$_2$ Monolayer towards SO$_2$, SOF$_2$, and HF Gases

Aijuan Zhang [1], Qunfeng Dong [1], Yingang Gui [2,*], Jinfang Li [1] and Feng Wan [1]

[1] College of Physics and Electronic Engineering, Xianyang Normal University, Xianyang 712000, China; zhangaijuan2019@163.com (A.Z.); qunfengdong1028@163.com (Q.D.); lijinfang928@163.com (J.L.); wanfeng1101@163.com (F.W.)

[2] College of Engineering and Technology, Southwest University, Chongqing 400715, China

* Correspondence: yinganggui@swu.edu.cn

Abstract: Detecting the characteristic decomposition products (SO$_2$, SOF$_2$, and HF) of SF$_6$ is an effective way to diagnose the electric discharge in SF$_6$-insulated equipment. Based on first-principles calculations, Au, Ag, and Cu were chosen as the surface modification transition metal to improve the adsorption and gas-sensing properties of MoTe$_2$ monolayer towards SO$_2$, SOF$_2$, and HF gases. The results show that Au, Ag, and Cu atoms tend to be trapped by T$_H$ sites on the MoTe$_2$ monolayer, and the binding strength increases in the order of Ag < Au < Cu. In gas adsorption, the moderate adsorption energy provides the basis that the TM-MoTe$_2$ monolayer can be used as gas-sensing material for SO$_2$, SOF$_2$, and HF. The conductivity of the adsorption system changes significantly. The conductivity decreases upon gases adsorption on TM-MoTe$_2$ monolayer, except the conductivity of Ag-MoTe$_2$ monolayer increases after interacting with SOF$_2$ gas.

Keywords: MoTe$_2$ monolayer; SO$_2$; SOF$_2$; HF; DFT

1. Introduction

In the compact design of high-voltage equipment and gas insulation systems in the power industry [1], SF$_6$ gas has been widely used as an insulation medium due to its comprehensive advantages, such as high dielectric strength, strong electronegativity, thermal stability, chemical inertness, and non-toxicity [2,3]. However, SF$_6$ gas inevitably decomposes to toxic and corrosive by-products under electric discharge [4]. Corona, spark, and arc discharge are three typical types of electric discharge observed in SF$_6$-insulated equipment [5]. Under the electric discharge, the low-sulfur fluorides produced by ionizing SF$_6$ gas will quickly react with trace moisture and impurities in the gas insulation system, forming some common stable decomposition products, including SO$_2$, SOF$_2$, and HF [6–8]. If these decomposition products are not handled properly, they will reduce the insulation strength of the filling gas, and be harmful to the environment and human health [9]. In addition, these acid gases will also corrode the original insulation device inside the gas insulation system, aggravating electric discharge and further affecting the safe and stable operation of the power system [10]. Online detection of the concentration of SO$_2$, SOF$_2$, and HF gases in the gas insulation system is crucial to ensure the safe running of equipment [11]. Therefore, it is urgent to explore suitable gas-sensitive materials for high-efficiency detection of the SF$_6$ decomposed gases.

Based on the catalytic performance and unique electrical structure, two-dimensional layered materials-based chemical sensors have been extensively explored and studied in broad application prospects, such as equipment testing, environmental diagnosis, and industrial manufacturing [12,13]. Graphene-like materials, such as transition metal dihalides (TMD), InN monolayers, hexagonal boron nitride (h-BN), and carbon nitride compounds, have a large specific surface area, and are resistant to strong acids and alkalis, and high temperatures [14–16]. Its adsorption and gas-sensitivity properties to gases have been

extensively studied [17,18]. Compared with other TMD, MoTe$_2$ has lower binding energy and a larger bond length [19,20]. TMD-based gas sensors have attracted broad focus in recent years [21]. Wang et al. studied the gas-sensing potential of MoTe$_2$ monolayer to SF$_6$ decomposition products based on theoretical calculations [22]. Feng et al. developed a MoTe$_2$-based gas sensor for NH$_3$ and NO$_2$ detection, with an excellent recovery rate and high sensitivity [23]. These previous studies have significantly enhanced the chemical interaction with specific gases, providing a promising candidate for SF$_6$ decomposition product detection.

The introduction of transition metal atom modification on the surface of two-dimensional layered materials effectively improves surface activity and gas-sensing performance [24,25]. In particular, nano-noble metals, such as Au, Ag, and Cu, may show better surface performance [26]. This is because transition metal atom modification increase the chemical activity and electron mobility of pristine materials, opening up a new perspective on exploring high-performance gas sensor [27]. Based on density functional theory (DFT) calculations, transition metals (Au, Ag, and Cu) were selected as modifying atoms on the MoTe$_2$ surface in this study. Then, SO$_2$, SOF$_2$, and HF gas molecules are adsorbed on three transition metals (Au, Ag, and Cu) modified MoTe$_2$ monolayer, abbreviated as TM-MoTe$_2$. The surface modification and gas-sensing mechanism have been studied by analyzing the geometric structures and electronic properties.

2. Computational Details

All calculations are performed based on DFT calculations [28]. The Perdew–Burke–Ernzerhof (PBE) function of the generalized gradient approximation method (GGA) was selected to approximate the exchange and correlation of electrons [29]. DFT Semi-core Pseudopot (DSPP) was selected to eliminate the relativistic effect of TM atoms in the core processing [30]. The p-orbital dual-value plus polarization function (DNP) was used as the atomic orbital basis set, which increases the calculation accuracy of hydrogen bonds [31]. The Grimme method performed DFT-D correction on Ag and Cu modified MoTe$_2$ models. While DFT-D2 method by TS was used to analyze the intermolecular forces and long-range interactions in the Au-modified MoTe$_2$ model.

A $7 \times 7 \times 1$ Monkhorst pack grid was wet for Brillouin sampling. A static calculation with a self-consistent field convergence accuracy of 10^{-6} Ha, a global orbit cut-off radius of 4.9 Å, and a smearing of 0.005 Ha were used to ensure the smooth convergence of the entire system [32]. According to the principle of periodic boundary conditions to eliminate the boundary effect, a single layer of MoTe$_2$ was constructed in a $4 \times 4 \times 1$ supercell containing 16 Mo atoms and 32 Te atoms. A vacuum interval of 20 Å is used to avoid mutual influence between adjacent layers [33]. Four possible modification sites of TM atoms on MoTe$_2$ were considered, including T$_H$, T$_{Mo}$, T$_{Te}$, and T$_B$. T$_H$ is the location above the center of the MoTe$_2$ hexagonal ring, T$_{Mo}$ is the location on the top of the Mo atom, T$_{Te}$ is the location on the top of the Te atom, and T$_B$ means the location on the bridge between two Te atoms. The binding energy (E_b) of TM atoms on the MoTe$_2$ monolayer is defined in Equation (1). Where $E_{TM-MoTe2}$, E_{TM}, and E_{MoTe2} represent the energy of TM-MoTe$_2$ monolayer, TM atom, and pristine MoTe$_2$ monolayer, respectively.

$$E_b = E_{TM\text{-}MoTe2} - E_{TM} - E_{MoTe2} \tag{1}$$

After obtaining the most stable TM-MoTe$_2$ monolayer structure, various possible adsorption positions of the gas molecule on TM-MoTe$_2$ were considered to study the adsorption behavior. Gas molecules undergo significant displacement and move to the highest stability position after structural optimization. The most stable configuration for gas molecule adsorption is determined by the largest adsorption energy (E_{ads}) calculated as Equation (2):

$$E_{ads} = E_{TM\text{-}MoTe2/gas} - E_{TM\text{-}MoTe2} - E_{gas} \tag{2}$$

where $E_{\text{TM-MoTe2/gas}}$ is the total energy of the adsorption system, while $E_{\text{TM-MoTe2}}$ and E_{gas} are the total energy of separated TM-MoTe$_2$ monolayer and gas molecules, respectively. The Mulliken atomic charges method is used to analyze the charge transfer. A negative value of charge transfer indicates the electrons transfer from TM-MoTe$_2$ monolayer to gas molecules.

3. Results and Discussion

3.1. Structural Optimization of Gas Molecules and TM-MoTe$_2$ Monolayer

As shown in Figure 1, the pristine MoTe$_2$ monolayer, TM atoms, SO$_2$, SOF$_2$, and HF gas molecules were optimized. The pristine MoTe$_2$ monolayer structure is composed of a hexagonal pattern with Se atoms and Mo atoms intersecting. The Mo-Te bond length of the MoTe$_2$ monolayer structure before TM modification is 2.758 Å. SO$_2$ gas molecule has a broken-line spatial configuration, which structure keeps good agreement with the reported theoretical and experimental results. The central S atom and the other two O atoms are bonded by σ bonds, and the O-S-O structure forms an angle of 119.954° and an S-O bond length of 1.480 Å. SOF$_2$ gas molecules belong to a three-dimensional structure due to the multiple-valence property. The bond lengths of the S-F bond and the S-O bond are 1.670 Å and 1.461 Å, respectively, and the angles of the O-S-F structure and the F-S-F structure are 107.175° and 93.297°, respectively. HF gas is in a linear structure with a bond length of 0.932 Å.
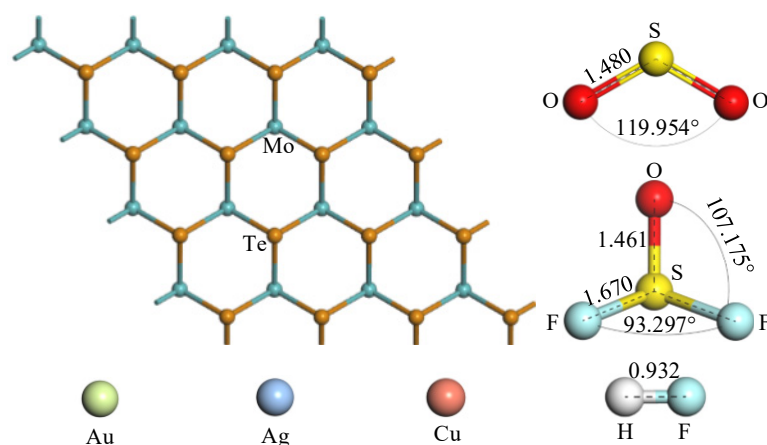

Figure 1. The optimized structures of the pristine MoTe$_2$, TM atoms, SO$_2$, SOF$_2$, and HF gases. The unit is Å.

First, the geometric structure and electronic properties of the TM-MoTe$_2$ monolayer were studied. Liu et al. achieved geometric relaxation of TM modification on the pristine MoTe$_2$ monolayer through four possible positions [34]. After complete optimization, it can be seen that the TM atoms prefer to be trapped at the TH site (located above the center of the MoTe$_2$ hexagonal ring). Therefore, this paper has three different TM atoms in the TH position for geometric optimization. It is worth noting that the three TM atoms form three bonds with three adjacent Te atoms after optimization, resulting in a certain degree of structural distortion in each system. However, in the optimized configuration, the lengths of the three TM-Te bonds are equal. It can be seen from Figure 2 that the average length of the TM-Mo bond in the TM-MoTe$_2$ model is 2.942 Å, 2.974 Å, and 2.618 Å, respectively.
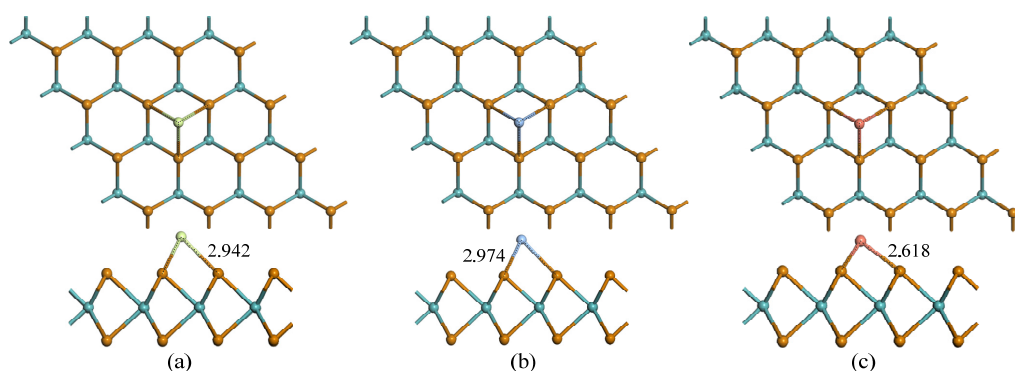
Figure 2. Top view and side view of: (**a**) Au-MoTe$_2$; (**b**) Ag-MoTe$_2$; (**c**) Cu-MoTe$_2$. The unit is Å.

Table 1 shows that the bonding strengths of TM atoms on MoTe$_2$, which increase in the order of Ag < Au < Cu, and the binding energies are 1.61 eV, 1.47 eV, and 1.13 eV, respectively. It shows that Au, Ag, and Cu of the same group can interact with the adjacent undercoordinated Mo atoms. The electron transfer from the TM atoms to the MoTe$_2$ monolayer is −0.238 e, 0.007 e, and −0.104 e, respectively, which is crucial to the chemical activity and sensitivity of the TM modified MoTe$_2$ monolayer. As shown in Figure 3, the band gaps of the MoTe$_2$ single layer under TS optimization and Grimme optimization are 1.273 eV and 1.275 eV, respectively, which is not much different overall. All of the bandgaps of the TM-MoTe$_2$ monolayer reduce, especially the bandgap of Au-MoTe$_2$ reduces to 0.728 eV. The band gaps of Ag-MoTe$_2$ and Cu-MoTe$_2$ are also respectively reduced to 0.794 eV and 0.838 eV, which is very important for the performance of the activated material.

Table 1. Binding energy and charge transfer of TM atoms modification on MoTe$_2$.

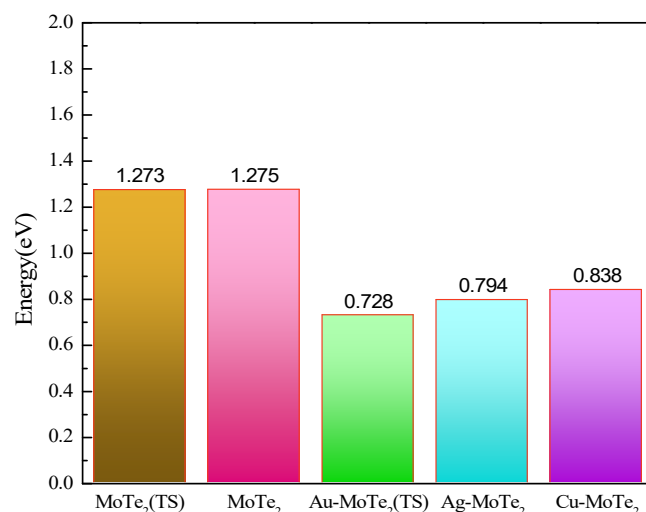| Modification Site	E_{bind} (eV)	Q_T (e)
Au-MoTe$_2$	−1.47	−0.238
Ag-MoTe$_2$	−1.13	0.007
Cu-MoTe$_2$	−1.61	−0.104

Figure 3. The bandgaps of the pristine MoTe$_2$ monolayer and TM-MoTe$_2$ monolayer.

3.2. Adsorption of Gas Molecules on TM-MoTe$_2$ Monolayer

The adsorption structures of SO$_2$, SOF$_2$, and HF gas molecules on the most stable TM-MoTe$_2$ monolayer structure were obtained, as shown in Figure 4. Table 2 lists the adsorption energy and charge transfer between the TM-MoTe$_2$ adsorption system and SO$_2$, SOF$_2$, and HF gas molecules. The calculated E_{ads} ranges from −0.23 eV to −1.18 eV,

determining whether gas adsorption processes belong to chemical or physical adsorption. Q_T ranges from +0.031 e to −0.341 e, indicating the redistribution of the electrons for all systems. It can be seen that SOF_2 prefers to interact with the TM-$MoTe_2$ monolayer by the S atom of SO_2F_2 approaching the TM atom. This is because the unique molecular configuration of SOF_2 makes the S atom more multivalent.

Table 2. Adsorption energy and electron transfer of gas molecules on TM-$MoTe_2$ monolayer.

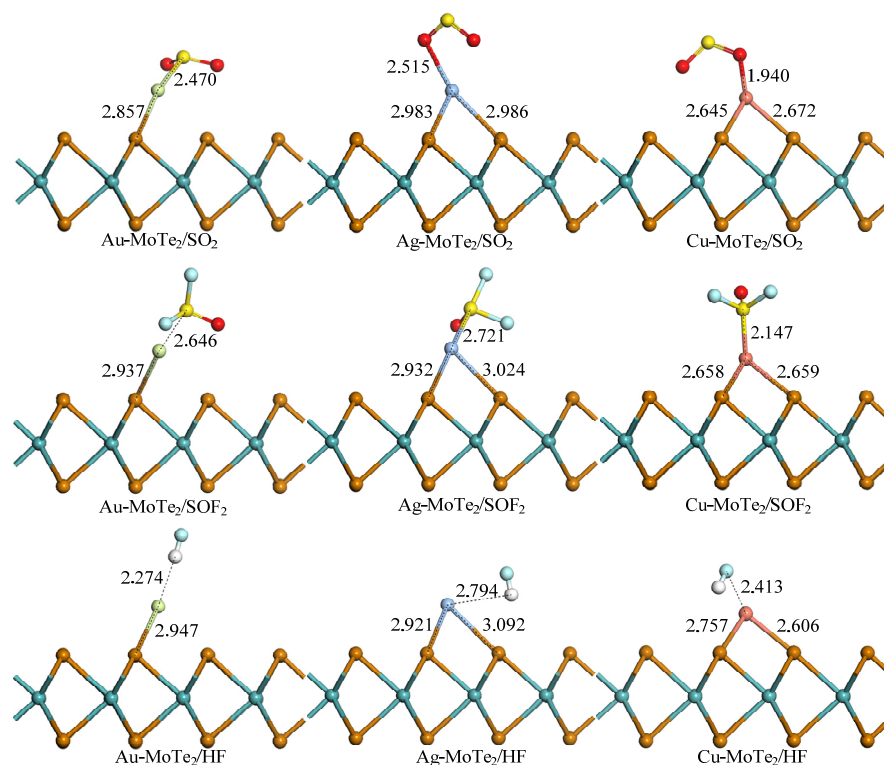| Parameters	E_{ads} (eV)	Q_T (e)
Au-$MoTe_2$/SO_2	−0.98	−0.259
Ag-$MoTe_2$/SO_2	−0.81	−0.341
Cu-$MoTe_2$/SO_2	−1.18	−0.316
Au-$MoTe_2$/SOF_2	−0.49	−0.147
Ag-$MoTe_2$/SOF_2	−0.4	−0.158
Cu-$MoTe_2$/SOF_2	−0.6	0.077
Au-$MoTe_2$/HF	−0.23	−0.033
Ag-$MoTe_2$/HF	−0.32	−0.007
Cu-$MoTe_2$/HF	−0.33	0.031

Figure 4. Adsorption systems of the gas molecule on TM-$MoTe_2$ monolayer. The unit is Å.

It can be seen from Figure 4 that the structure of the TM-$MoTe_2$ monolayer has undergone significant deformation after the adsorption of SO_2, SOF_2, and HF gas molecules. In particular, the Au atom undergoes a significant movement from the initial modification position, the position above the center of the $MoTe_2$ hexagonal ring to a position partial to the top of the Te atom, and two of the original three Au-Te bonds are broken. The length of the remained Au-Te bond changes to 2.857 Å, 2.937 Å, and 2.947 Å when SO_2, SOF_2, and HF gases adsorb on the Au-$MoTe_2$ monolayer, respectively. On the other hand, the Ag and Cu modified $MoTe_2$ monolayer have not undergone significant geometric deformation during the adsorption of SO_2, SOF_2, and HF gases, though the Ag-Te bond and Cu-Te bond are elongated to some extent. It can be determined that the Ag-$MoTe_2$ adsorption system is similar to the Cu-$MoTe_2$ adsorption system. The O atoms in the SO_2 gas molecule and the S atoms in the SOF_2 gas molecule are stably captured by the Ag atom and Cu atom by

forming corresponding chemical bonds: Ag-O (2.515 Å), Ag-S (2.721 Å), Cu-O (1.940 Å), and Cu-S (2.147 Å).

3.3. TDOS and PDOS Distribution of Gas Adsorbed TM-MoTe$_2$ Monolayer

Figure 5 shows the TDOS distribution of TM-MoTe$_2$ monolayers before and after SO$_2$, SOF$_2$, and HF gas adsorption. It can be seen that the TDOS distribution of the Au-MoTe$_2$ monolayer shifts to the right as a whole after the adsorption of SO$_2$, SOF$_2$, and HF gases, proving that the modification of Au atoms improves the chemical activity and conductivity of the adsorption system. In addition, due to the activated state of the adsorbed SOF$_2$ gas molecule, the TDOS distribution of the SOF$_2$ adsorbed TM-MoTe$_2$ system showed a continuous new peak between -10 eV and -5 eV. Moreover, the TDOS distribution of the SOF$_2$ gas adsorption system fluctuates the most in all distributions due to a certain amount of charge transfer during the adsorption process. On the right side of the Fermi level, the TDOS distribution decreases after SO$_2$ gas adsorption on the Ag-MoTe$_2$ monolayer and Cu-MoTe$_2$ monolayer, indicating that the filled electrons reduce, and a strong chemical effect occurs during the adsorption process. The TDOS distribution of the HF adsorbed Au-MoTe2 system shifts slightly to the right, but the TDOS distribution of the other two HF gas adsorption systems nearly does not change.
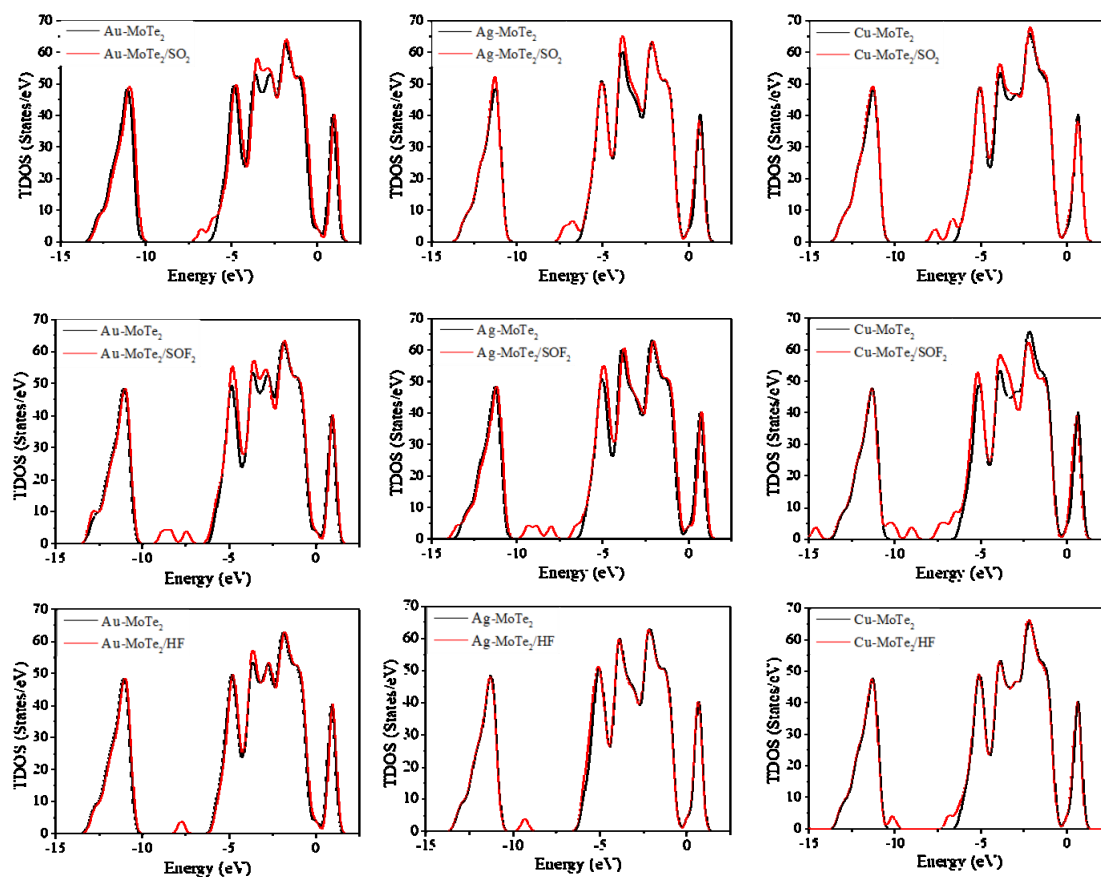

Figure 5. TDOS distribution of SO$_2$, SOF$_2$, and HF adsorbed TM-MoTe$_2$ systems.

PDOS analysis was performed to understand the electronic behavior of TM-MoTe$_2$ monolayer when adsorbing SO$_2$, SOF$_2$, and HF gases, as shown in Figure 6. It can be found that the 5*d*, 4*d* and 3*d* orbits of Au, Ag, and Cu atoms have a significant influence on their respective TDOS distributions due to their mental activities. It can be seen from the PDOS distribution of each adsorption system that the *d* orbits of TM atoms highly hybridize with the *p* orbits of S atoms or O atoms of the adsorbed SO$_2$ gas molecules and SOF$_2$ gas molecules. It confirms the stable formation of TM-S or TM-O bonds in the TM-MoTe$_2$

adsorption system. In the TDOS distribution of all TM-MoTe$_2$/HF adsorption systems, a slight fluctuation between -12.5 eV and -7.5 eV appears as a new peak derived from the 2*p* and 1*s* orbits of HF gas molecule. These orbital interactions indicate that SO$_2$, SOF$_2$, and HF gases have an ideal adsorption effect on the TM-MoTe$_2$ monolayer, which leads to the redistribution of electrons on the substrate and a change of conductivity to a large extent.
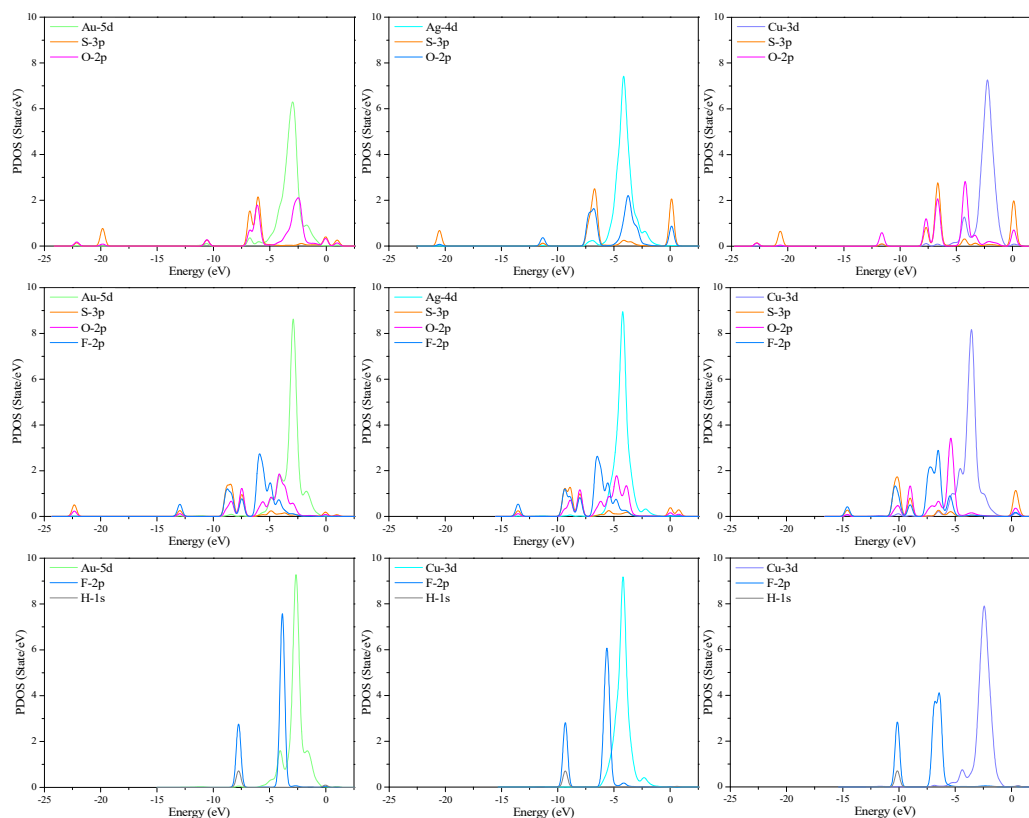

Figure 6. PDOS distribution of SO$_2$, SOF$_2$, and HF adsorbed TM-MoTe$_2$ systems.

3.4. Molecular Orbital Analysis of Gas Adsorbed TM-MoTe$_2$ Monolayer

The adsorption of SO$_2$, SOF$_2$, and HF gases on the TM-MoTe$_2$ monolayer was analyzed by molecular orbital analysis. According to the molecular orbital theory, the highest occupied molecular orbit (HOMO) and lowest unoccupied molecular orbit (LUMO) distributions of the adsorption system were calculated as shown in Figure 7. The yellow and blue areas in Figure 7 represent the positive and negative phases of the wave function. Table 3 shows the energy gap (E_g) between HOMO and LUMO, which helps evaluate the change in conductivity.

Molecular orbit is an effective method to evaluate the probability of electron transfer between characteristic molecules and the surface of TM-MoTe$_2$. This confirms the previous DOS analysis that SO$_2$, SOF$_2$, and HF gas molecules are non-magnetic molecules during adsorption. At the same time, the E_g of the TM-MoTe$_2$ monolayer changes after the gas molecules' adsorption. For the Ag-MoTe$_2$ system, the E_g of the adsorption system decreases after SOF$_2$ gas molecules adsorption. While for other TM-MoTe$_2$ systems, the E_g of the adsorption system increases after the gas adsorption. As the LUMO distribution obviously increases around the gas adsorption site, and HOMO distribution on Ag-MoTe$_2$ slightly increases when SOF$_2$ adsorption on the Ag-MoTe$_2$ system. As a result, the electron transition from HOMO to LUMO becomes easier, and E_g decreases simultaneously. Therefore, the conductivity of the Ag-MoTe$_2$ monolayer increases after interacting with SOF$_2$ gas, while the conductivity of other adsorption systems decreases. As shown in Figure 7, the adsorption of gas molecules causes the redistribution of electrons in TM-MoTe$_2$, which

changes the energy of HOMO and LUMO accordingly, which matches the changing trend of E_g.
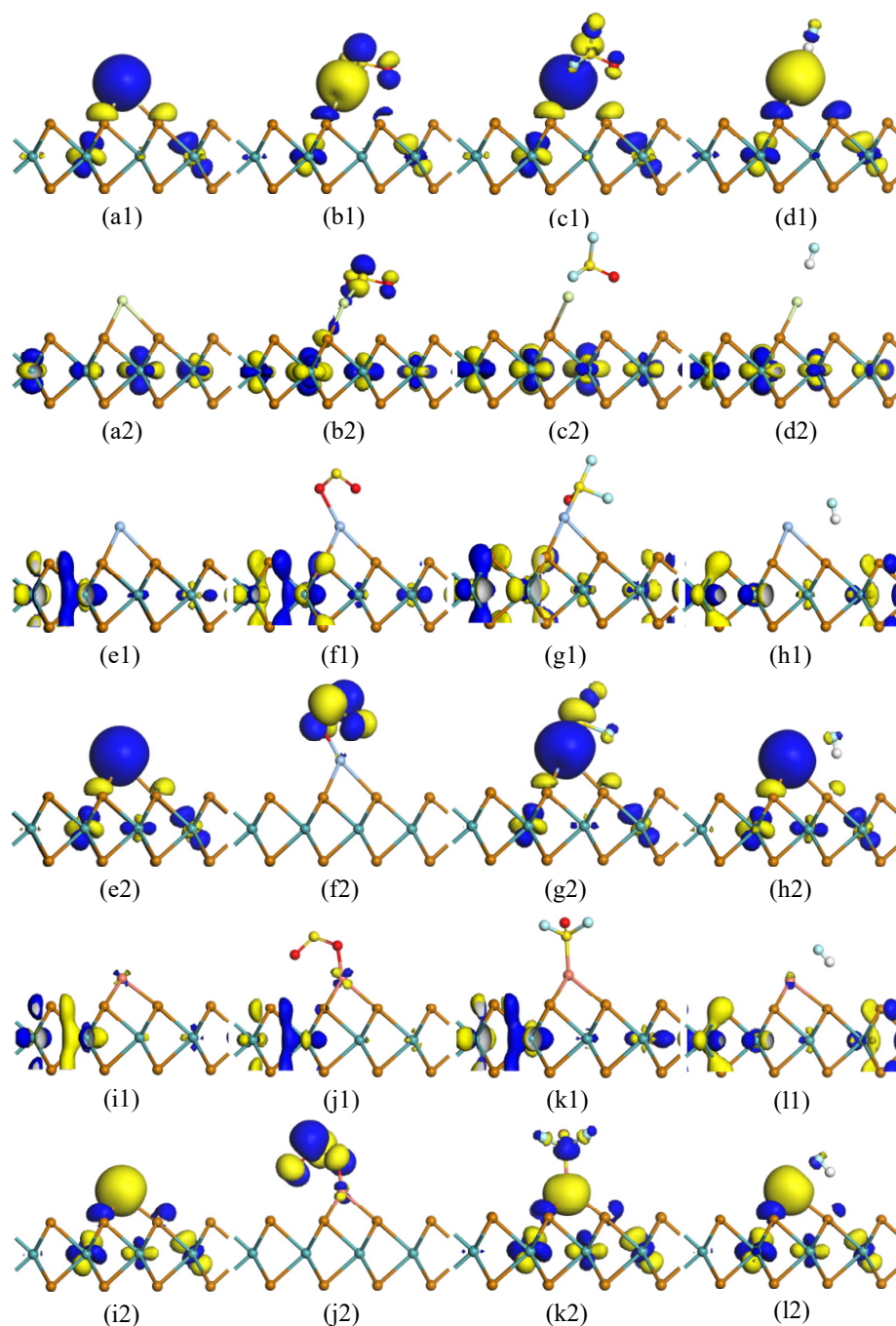

Figure 7. HOMO and LUMO distribution of TM-MoTe$_2$ monolayer before and after gas adsorption. (**a1**) Au-MoTe$_2$-HOMO, (**a2**) Au-MoTe$_2$-LUMO, (**b1**) Au-MoTe$_2$/SO$_2$-HOMO, (**b2**) Au-MoTe$_2$/SO$_2$-LUMO, (**c1**) Au-MoTe$_2$/SOF$_2$-HOMO, (**c2**) Au-MoTe$_2$/SOF$_2$-LUMO, (**d1**) Au-MoTe$_2$/HF-HOMO, (**d2**) Au-MoTe$_2$/HF-LUMO, (**e1**) Ag-MoTe$_2$-HOMO, (**e2**) Ag-MoTe$_2$-LUMO, (**f1**) Ag-MoTe$_2$/SO$_2$-HOMO, (**f2**) Ag-MoTe$_2$/SO$_2$-LUMO, (**g1**) Ag-MoTe$_2$/SOF$_2$-HOMO, (**g2**) Ag-MoTe$_2$/SOF$_2$-LUMO, (**h1**) Ag-MoTe$_2$/HF-HOMO, (**h2**) Ag-MoTe$_2$/HF-LUMO, (**i1**) Cu-MoTe$_2$-HOMO, (**i2**) Cu-MoTe$_2$-LUMO, (**j1**) Cu-MoTe$_2$/SO$_2$-HOMO, (**j2**) Cu-MoTe$_2$/SO$_2$-LUMO, (**k1**) Cu-MoTe$_2$/SOF$_2$-HOMO, (**k2**) Cu-MoTe$_2$/SOF$_2$-LUMO, (**l1**) Cu-MoTe$_2$/HF-HOMO, (**l2**) Cu-MoTe$_2$/HF-LUMO.

Table 3. Molecular orbits and energy gaps of before and after gas adsorption on TM-MoTe$_2$.

Adsorption Structure	E_{HOMO} (eV)	E_{LUMO} (eV)	E_g (eV)
Au-MoTe$_2$	−4.599	−3.646	0.953
Au-MoTe$_2$/SO$_2$	−4.898	−3.837	1.061
Au-MoTe$_2$/SOF$_2$	−4.844	−3.81	1.034
Au-MoTe$_2$/HF	−4.926	−3.891	1.035
Ag-MoTe$_2$	−5.143	−4.163	0.98
Ag-MoTe$_2$/SO$_2$	−5.333	−4.218	1.115
Ag-MoTe$_2$/SOF$_2$	−5.306	−4.435	0.871
Ag-MoTe$_2$/HF	−5.225	−4.191	1.034
Cu-MoTe$_2$	−5.17	−4.136	1.034
Cu-MoTe$_2$/SO$_2$	−5.306	−4.218	1.088
Cu-MoTe$_2$/SOF$_2$	−5.333	−4.136	1.197
Cu-MoTe$_2$/HF	−5.197	−4.082	1.115

4. Conclusions

Based on first-principles calculations, this paper studies the stable structure of TM (Au, Ag, and Cu) modification on the MoTe$_2$ monolayer. Then the adsorption structures of the characteristic decomposition products of SF$_6$ (SO$_2$, SOF$_2$, and HF) on the TM-MoTe$_2$ monolayer were calculated. By analyzing the adsorption structure, adsorption energy, charge transfer, adsorption distance, TDOS, PDOS, and molecular orbit, the adsorption performance and electronic behavior of TM-MoTe$_2$ monolayer towards SO$_2$, SOF$_2$, and HF gases were explored. TM atoms tend to be trapped by T$_H$ sites on the MoTe$_2$ monolayer with a binding strength of Ag <Au < Cu. The adsorption energy of the TM-MoTe$_2$ monolayer to SO$_2$, SOF$_2$, and HF gas is moderate, indicating that they are suitable gas-sensing materials for detecting SO$_2$, SOF$_2$, and HF gases. The adsorption of SO$_2$, SOF$_2$, and HF gases on the TM-MoTe$_2$ monolayer leads to the redistribution of electrons in the TM-MoTe$_2$ systems, affecting its conductivity to a large extent. After SOF$_2$ adsorption on the Ag-MoTe$_2$ monolayer, the conductivity increases along with the decreased E_g, while the other gas adsorption on the TM-MoTe$_2$ monolayer leads to an increase of E_g and a decrease in conductivity. Based on the different change rules of conductivity of the systems, it realizes the selective detection of the mixed decomposition products.

Author Contributions: Conceptualization, A.Z. and Y.G.; methodology, Y.G.; formal analysis, Q.D.; investigation, A.Z.; data curation, Y.G.; writing—original draft preparation, Y.G.; writing—review and editing, Y.G.; visualization, J.L.; supervision, A.Z.; project administration, A.Z.; funding acquisition, Q.D., J.L. and F.W. All authors have read and agreed to the published version of the manuscript.

Institutional Review Board Statement: Not applicable.

Informed Consent Statement: Not applicable.

Data Availability Statement: Not applicable.

Conflicts of Interest: The authors declare that they have no known competing financial interests or personal relationships that could have appeared to influence the work reported in this paper.

Sample Availability: Samples of the compounds are not available from the authors.

References

1. Xu, L.; Gui, Y.; Li, W.; Li, Q.; Chen, X. Gas-sensing properties of Ptn-doped WSe$_2$ to SF$_6$ decomposition products. *J. Ind. Eng. Chem.* **2021**, *97*, 452–459. [CrossRef]
2. Gui, Y.G.; Shi, J.Z.; Yang, P.A.; Li, T.; Tang, C.; Xu, L.N. Platinum modified MoS$_2$ monolayer for adsorption and gas sensing of SF6 decomposition products: A DFT study. *High Volt.* **2020**, *5*, 454–462. [CrossRef]
3. Cao, W.H.; Gui, Y.G.; Chen, T.; Xu, L.N.; Ding, Z.Y. Adsorption and gas-sensing properties of Pt2-GaNNTs for SF$_6$ decom-position products. *Appl. Surf. Sci.* **2020**, *524*, 146570. [CrossRef]
4. Zhang, X.X.; Yu, L.; Wu, X.Q.; Hu, W.H. Experimental Sensing and Density Functional Theory Study of H$_2$S and SOF$_2$ Ad-sorption on Au-Modified Graphene. *Adv. Sci.* **2015**, *2*, 1500101. [CrossRef]
5. Chu, J.; Li, W.; Yang, X.; Wu, Y.; Wang, D.; Yang, A.; Yuan, H.; Wang, X.; Li, Y.; Rong, M. Identification of gas mixtures via sensor array combining with neural networks. *Sens. Actuators B Chem.* **2020**, *329*, 129090. [CrossRef]
6. Zhang, J.; Zhu, W.; Chen, D.; Li, K.; Zhang, Q.; Wang, X.; Zheng, X.; Jiang, L.; Cao, L.; Lingzhi, C. Effects of remanent magnetization on dynamic magnetomechanical and magnetic-sensing characteristics in bi-layer multiferroics. *Eur. Phys. J. Appl. Phys.* **2019**, *85*, 20601. [CrossRef]
7. Yang, A.; Wang, D.; Lan, T.; Chu, J.; Li, W.; Pan, J.; Liu, Z.; Wang, X.; Rong, M. Single ultrathin WO$_3$ nanowire as a superior gas sensor for SO$_2$ and H$_2$S: Selective adsorption and distinct I-V response. *Mater. Chem. Phys.* **2019**, *240*, 122165. [CrossRef]
8. Chen, D.; Zhang, X.; Tang, J.; Cui, H.; Li, Y. Noble metal (Pt or Au)-doped monolayer MoS2 as a promising adsorbent and gas-sensing material to SO$_2$, SOF$_2$ and SO$_2$F$_2$: A DFT study. *Appl. Phys. A* **2018**, *124*, 194. [CrossRef]
9. Cui, H.; Zhang, X.; Zhang, G.; Tang, J. Pd-doped MoS$_2$ monolayer: A promising candidate for DGA in transformer oil based on DFT method. *Appl. Surf. Sci.* **2018**, *470*, 1035–1042. [CrossRef]
10. Cui, H.; Zhang, X.; Li, Y.; Chen, D.; Zhang, Y. First-principles insight into Ni-doped InN monolayer as a noxious gases scavenger. *Appl. Surf. Sci.* **2019**, *494*, 859–866. [CrossRef]
11. Hu, X.; Gui, Y.; Liu, Y.; Xu, L.; Ran, L.; Chen, X. Adsorption characteristics of H$_2$S, SO$_2$, SO2F$_2$, SOF$_2$, and N$_2$ on NiO-MoSe$_2$ monolayer for gas-sensing applications. *Vacuum* **2021**, *193*, 110506. [CrossRef]
12. Zhang, J.; Chen, D.; Filippov, D.A.; Geng, S.; Li, K.; Zhang, Q.; Jiang, L.; Wang, X.; Zhu, W.; Cao, L.; et al. Theory of tunable magnetoelectric inductors in ferrite-piezoelectric layered composite. *J. Phys. D Appl. Phys.* **2019**, *52*, 165001. [CrossRef]
13. Ou, J.Z.; Ge, W.; Carey, B.; Daeneke, T.; Rotbart, A.; Shan, W.; Wang, Y.; Fu, Z.; Chrimes, A.F.; Wlodarski, W.; et al. Physisorption-Based Charge Transfer in Two-Dimensional SnS$_2$ for Selective and Reversible NO$_2$ Gas Sensing. *ACS Nano* **2015**, *9*, 10313–10323. [CrossRef] [PubMed]
14. Gui, Y.G.; Peng, X.; Liu, K.; Ding, Z.Y. Adsorption of C$_2$H$_2$, CH$_4$ and CO on Mn-doped graphene: Atomic, electronic, and gas-sensing properties. *Phys. E-Low-Dimens. Syst. Nanostruct.* **2020**, *119*, 113959. [CrossRef]
15. Cui, H.; Zhang, G.; Zhang, X.; Tang, J. Rh-doped MoSe$_2$ as a toxic gas scavenger: A first-principles study. *Nanoscale Adv.* **2018**, *1*, 772–780. [CrossRef]
16. Cui, H.; Chen, D.; Zhang, Y.; Zhang, X. Dissolved gas analysis in transformer oil using Pd catalyst decorated MoSe$_2$ monolayer: A first-principles theory. *Sustain. Mater. Technol.* **2019**, *20*, e00094. [CrossRef]
17. Liu, H.; Xu, L.N.; Gui, Y.G.; Ran, L.; Chen, X.P. Adsorption properties of Ag$_2$O-MoSe$_2$ towards SF$_6$ decomposed products. *Vacuum* **2021**, *189*, 110248. [CrossRef]
18. Zhang, D.Z.; Jiang, C.X.; Wu, J.F. Layer-by-layer assembled In$_2$O$_3$ nanocubes/flower-like MoS$_2$ nanofilm for room temper-ature formaldehyde sensing. *Sens. Actuator B-Chem.* **2018**, *273*, 176–184. [CrossRef]
19. Gui, Y.; Shi, J.; Xu, L.; Ran, L.; Chen, X. Au (n = 1–4) cluster doped MoSe$_2$ nanosheet as a promising gas-sensing material for C$_2$H$_4$ gas in oil-immersed transformer. *Appl. Surf. Sci.* **2021**, *541*, 148356. [CrossRef]
20. Ma, Y.; Dai, Y.; Guo, M.; Niu, C.; Lu, J.; Huang, B. Electronic and magnetic properties of perfect, vacancy-doped, and nonmetal adsorbed MoSe$_2$, MoTe$_2$ and WS$_2$ monolayers. *Phys. Chem. Chem. Phys.* **2011**, *13*, 15546–15553. [CrossRef]
21. Yang, P.-A.; Ruan, H.; Sun, Y.; Li, R.; Lu, Y.; Xiang, C. Excellent microwave absorption performances of high length-diameter ratio iron nanowires with low filling ratio. *Nanotechnology* **2020**, *31*, 395708. [CrossRef] [PubMed]
22. Wang, D.W.; Wang, X.H.; Yang, A.J.; Chu, J.F.; Lv, P.L.; Liu, Y.; Rong, M.Z. MoTe2: A Promising Candidate for SF$_6$ De-composition Gas Sensors With High Sensitivity and Selectivity. *IEEE Electron Device Lett.* **2018**, *39*, 292–295. [CrossRef]
23. Feng, Z.; Xie, Y.; Chen, J.; Yu, Y.; Zheng, S.; Zhang, R.; Li, Q.; Chen, X.; Sun, C.; Zhang, H.; et al. Highly sensitive MoTe$_2$ chemical sensor with fast recovery rate through gate biasing. *2D Mater.* **2017**, *4*, 025018. [CrossRef]
24. Yagi, Y.; Briere, T.M.; Sluiter, M.H.F.; Kumar, V.; Farajian, A.A.; Kawazoe, Y. Stable geometries and magnetic properties of single-walled carbon nanotubes doped with 3d transition metals: A first-principles study. *Phys. Rev. B* **2004**, *69*, 075414. [CrossRef]
25. Zhang, D.; Jiang, C.; Liu, J.; Cao, Y. Carbon monoxide gas sensing at room temperature using copper oxide-decorated graphene hybrid nanocomposite prepared by layer-by-layer self-assembly. *Sens. Actuators B Chem.* **2017**, *247*, 875–882. [CrossRef]
26. Yuwen, L.H.; Xu, F.; Xue, B.; Luo, Z.M.; Zhang, Q.; Bao, B.Q.; Su, S.; Weng, L.X.; Huang, W.; Wang, L.H. General synthesis of noble metal (Au, Ag, Pd, Pt) nanocrystal modified MoS2 nanosheets and the enhanced catalytic activity of Pd-MoS$_2$ for methanol oxidation. *Nanoscale* **2014**, *6*, 5762–5769. [CrossRef] [PubMed]
27. Lin, S.; Ye, X.; Johnson, R.S.; Guo, H. First-Principles Investigations of Metal (Cu, Ag, Au, Pt, Rh, Pd, Fe, Co, and Ir) Doped Hexagonal Boron Nitride Nanosheets: Stability and Catalysis of CO Oxidation. *J. Phys. Chem. C* **2013**, *117*, 17319–17326. [CrossRef]

28. Li, X.; Tang, C.; Wang, J.; Tian, W.; Hu, D. Analysis and mechanism of adsorption of naphthenic mineral oil, water, formic acid, carbon dioxide, and methane on meta-aramid insulation paper. *J. Mater. Sci.* **2019**, *54*, 8556–8570. [CrossRef]

29. He, X.; Gui, Y.; Liu, K.; Xu, L. Comparison of sensing and electronic properties of C2H2 on different transition metal oxide nanoparticles (Fe$_2$O$_3$, NiO, TiO$_2$) modified BNNT (10, 0). *Appl. Surf. Sci.* **2020**, *521*, 146463. [CrossRef]

30. Chen, W.L.; Gui, Y.G.; Li, T.; Zeng, H.; Xu, L.N.; Ding, Z.Y. Gas-sensing properties and mechanism of Pd-GaNNTs for air decomposition products in ring main unit. *Appl. Surf. Sci.* **2020**, *531*, 147293. [CrossRef]

31. Zheng, W.; Tang, C.; Xie, J.F.; Gui, Y.G. Micro-scale effects of nano-SiO$_2$ modification with silane coupling agents on the cellulose/nano-SiO2 interface. *Nanotechnology* **2019**, *30*, 445701. [CrossRef] [PubMed]

32. Li, P.; Hong, Q.Y.; Wu, T.; Cui, H. SOF$_2$ sensing by Rh-doped PtS$_2$ monolayer for early diagnosis of partial discharge in the SF$_6$ insulation device. *Mol. Phys.* **2021**, *119*, e1919774. [CrossRef]

33. Zhou, Y.; Reed, E.J. Structural Phase Stability Control of Monolayer MoTe$_2$ with Adsorbed Atoms and Molecules. *J. Phys. Chem. C* **2015**, *119*, 21674–21680. [CrossRef]

34. Liu, Y.; Shi, T.; Si, Q.; Liu, T. Adsorption and sensing performances of transition metal (Pd, Pt, Ag and Au) doped MoTe$_2$ monolayer upon NO$_2$: A DFT study. *Phys. Lett. A* **2020**, *391*, 127117. [CrossRef]